4th International Conference on Earthquake Engineering
Taipei, Taiwan
October 12-13, 2006

Paper No. 027

RESPONSE OF RENYI-TAN DAM DURING THE 921- JIJI EARTHQUAKE

Meen-Wah Gui[1] and Hsien-Te Chiu[2]

ABSTRACT

Taiwan is located in one of the world earthquake-active zones, i.e. at the junction of the Manila and Ryukyu trenches in the Western Philippine Sea. In 1999, a devastating 921-JiJi earthquake struck Taiwan and caused severe properties losses and claimed thousands of lives. In addition, excessive ground deformation also caused severe cracks to the nearby Shi Gang concrete dam and caused the dam to completely losses its ability to retain water. This has resulted in a series of dam safety assessment from both the government agencies and research institutions in Taiwan. This study examined the behavior of Renyi-Tan earth dam during this JiJi earthquake. A series of numerical analyses treating the dam materials to obey Finn's model has been performed using the finite difference program FLAC. The numerical results were presented and evaluated from the viewpoint of displacement, excess pore pressure, stress path, and accelerations. The results showed that the dam was still intact during the JiJi earthquake because the generated excess pore water pressures in the dam body were only about 60% of its effective overburden stress, which inhibited the dam from liquefaction.

Keywords: dynamic response, numerical analysis, earth dam, excess pore-water pressure

INTRODUCTION

Taiwan has more than 50 dams with heights greater than 15 m and the common forms of these dams are concrete gravity dam, concrete arch dam and earth dam, in which 33 or them are earth-dams. The majority of these earth-dams were rolling type earth-dam with a clay core to prevent seepage of water from the upstream. Because Taiwan is located on the Circum-Pacific Seismic Zone, earthquake poses a very big threat to the safety of the dams and villagers around the areas. At 01:47 a.m. September 21, 1999, a strong earthquake with magnitude 7.3 struck Nantou County and inflicted severe damages to many parts of Taiwan. The earthquake caused 2,321 death and more than 8,000 people injured. The estimated properties lost were NT. 300 billions dollars. The earthquake focused beneath the city of JiJi at a depth of about 7-10 kilometers and many nearby dams received the shock. A concrete arch dam (Shigang dam), which is near the Chelong-Pu fault, suffered severe ground heaved, sheared-off and lost its capability of water storing. Some of the tourism spots around another nearby ReYe-Tan dam were also found destroyed. Shuishe dam and Toushe dam generated crack of about 100 m long as a result of uneven heave and subsidence. After this earthquake, engineers in Taiwan begin to focus on the earthquake response of the other dams in Taiwan.

It is highly essential to understand the earthquake response and evaluate the safety of earth-dams (Rizendiz et al., 1982). International Committee on Large Dams (ICOLD, 1979) investigated dams with height greater than 15 m, and found that 50% of the destroyed dams had height between 15 m to

[1] Civil Eng Dept (NTUT 2656), NTUT, No 1, Sec 3, ZhongXiao E Rd, Taipei 10608, Taiwan. Email: mwgui@ntut.edu.tw
[2] Formerly Civil Eng Dept, NTUT, No 1, Sec 3, ZhongXiao E Rd, Taipei 10608, Taiwan.

20 m. They also found that arch and gravity dams are the safest and second safest dams, respectively. Earth dams constituted 58% of all forms of built dams but 74% of failed dams were earth-dam. This study aims to understand the dynamic behavior of Renyi-Tan dam during the 921-earthquake. Dynamic analysis was carried out using the program FLAC. The phreatic surface in the dam was first determined prior to the dynamic analysis. For the dynamic analysis, the acceleration input is obtained from the x-acceleration history recorded during the 921-earthquake some 2 km away at WuFeng Primary School. The dynamic behavior of the dam is evaluated in terms of dam displacement, excess pore water pressure, and acceleration recorded throughout the depth of the dam.

BACKGROUND

Renyi-Tan Dam

Chia-Yi government started planning the Renyi-Tan dam in 1979 as a result of rapid industrial development and fast population increase, which in turns rapidly increase the demand of water consumption. Prior to this, the livelihood of the local community and industry depended on the underground water and the already undersupplied Lan-Tan dam, which located at about 2.1 km away. Construction of Renyi-Tan dam at the upstream of the Ba-Zhang River began in 1980 and it was completed in 1987. Renyi-Tan dam is an off-stream dam; its height is 29 m with a crest width of 9 m. The dam is 1535 m long with a water-storage area of about 3.66 km^2; the total water-storage capacity is about 29.11 million m^3, of which the effective water-storage capacity is 27.31 million m^3. Figure 1 shows a simplified cross-sectional of Renyi-Tan dam.

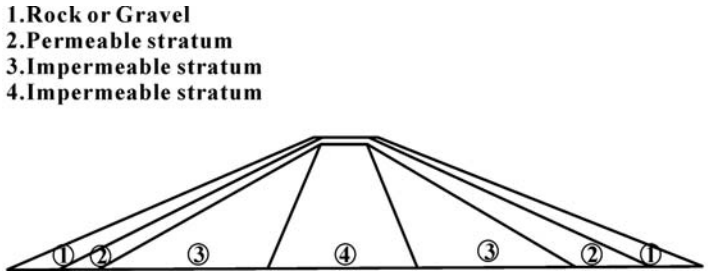

Figure 1. A simplified cross-sectional area of Renyi-Tan dam.

Geology of Renyi-Tan Dam

The dam is founded on the Pliocene to the Pleistocene Toukoshan formation and modern alluvium. The Toukoshan formation is exposed and is mainly made up of pale green to gray mud siltstone, sandstone and mudstone that formed the sedimentary rock of the environment on the brink of the sea. According to the geological drilling data, there is a ridge (top of the mountain) directed from the north and south, and the soil stratums can be divided from the top into alluvium, silty sandstone (silty sand/clay), sandstone (silty sand) and mudstone (batholith), respectively.

NUMERICAL MODELLING

FLAC (Fast Lagrangian Analysis of Continua) is a finite difference program commonly used in geotechnical and mining engineering. In the analysis, the program divides the geometry of the dam into small elements via several grid lines. The elements behave according to a prescribed linear or non-linear stress/strain law in response to the applied forces or boundary restrains. The advantage of using FLAC for seismic analysis is the simplicity of applying seismic loading anywhere within the problem domain and the excellent post-processing capabilities (Itasca Consulting Group, Inc., 2002).

Soil Model

Coupled dynamic-groundwater flow calculations can be performed with Finn model in FLAC2D (Itasca Consulting Group, Inc., 2002). Many researchers used it to analyze dynamic cases and the

results were closed to actual condition. For examples, Hsu et al. (2003) successfully simulated the lateral spread of soil in Wu-Feng after the JiJi earthquake and Lee (2000) also successfully modeled the earthquake-induced liquefaction of backfill behind caisson-type quay walls. Finn model (Itasca Consulting Group, Inc., 2002) adopted the pore pressure build-up mechanism proposed by Martin et al. (1975). Martin et al (1975) analyzed many drained dynamic shear tests that were tested by Silver and Seed (1971) and discovered the irrecoverable volume-strain relationship with cyclic shear-strain amplitude, which is independent of confining stress. Martin et al. (1975) supplied the relationship between decreased volumes of drained cyclic loading test and pore pressure rise of undrained test as follows:

Undrained condition

In the cyclic shear test, the changed of pore volume in each cycle is:

$$\frac{\Delta u n_p}{K_w} \tag{1}$$

where Δu = increment of pore water pressure in each cycle; K_w = bulk modulus of water; and n_p = porosity of soil. However, the changed of pore volume in each cycle can be regarded as the decreased of volume-strain where sand structure slides subtract the increased of recuperative soil-volume, $\Delta u/E_r$; thus

$$\frac{\Delta u n_p}{K_w} = \Delta\varepsilon_{vd} - \frac{\Delta u}{E_r} \quad or \quad \Delta u = \frac{\Delta\varepsilon_{vd}}{\frac{1}{E_r} + \frac{n_p}{K_w}} \tag{2}$$

where ε_{vd} = decreased of volume-strain where sand structure slides; and E_r = reloading modulus. If the degree of saturation is 100%, the water is usually regarded as uncompressible. So, Eq (2) can now be modified as:

$$\Delta\varepsilon_{vd} = \frac{\Delta u}{E_r} \quad or \quad \Delta u = E_r \Delta\varepsilon_{vd} \tag{3}$$

Drained condition

Martin et al. (1975) proposed the relationship between volume-strain and cyclic shear-strain amplitude of many drained cyclic shear tests as follows:

$$\Delta\varepsilon_{vd} = c_1\left(\gamma - c_2\varepsilon_{vd}\right) + \frac{c_3\varepsilon_{vd}^2}{\gamma + c_4\varepsilon_{vd}} \tag{4}$$

where γ = cyclic shear-strain amplitude; ε_{vd} = accumulated irrecoverable volume strain; and c_1, c_2, c_3, c_4 = constants. Martin et al (1975) performed regression on the data of tests, and derived the best c_1=0.8, c_2=0.79, c_3=0.45, c_4=0.73 parameters. The dissipated excess pore water is represented by:

$$\frac{\partial u}{\partial t} = E_r \frac{\partial}{\partial z}\left(\frac{k}{\gamma_w}\frac{\partial u}{\partial z}\right) + E_r \frac{\partial\varepsilon_{vd}}{\partial t} \tag{5}$$

where u = pore water pressure; k = permeability; γ_w = water density; z = depth; and t = time. The variation of pore water pressure causes the variation of effective stress, and the shear modulus of soil is also varied. The relationship between shear modulus, accumulated volume strain and effective stress where

$$G_{mn} = G_{m0}\left(1 + \frac{\varepsilon_{vd}}{H_1 + H_2\varepsilon_{vd}}\right)^s \frac{\sigma'_v}{\sigma'_{v0}} \quad and \quad \tau_{mn} = \tau_{m0}\left(1 + \frac{\varepsilon_{vd}}{H_3 + H_4\varepsilon_{vd}}\right)^s \frac{\sigma'_v}{\sigma'_{v0}} \qquad (6)$$

where G_{mn} = original shear module of n cycle; G_{m0} = original shear module; τ_{mn} = maximum shear stress of n cycle; τ_{m0} = original shear stress; and H_1, H_2, H_3, H_4=constants.

Materials Properties

In 1985, Taiwan Water Corporation appointed National Taiwan Institute of Technology (NTIT, 1987) to conduct soil elements tests for two of the sections of the dam. The tests included: (i) physical properties (specific gravity, water content, sieve analysis, liquid limit and plastic limit); (ii) unsaturated unconsolidated undrained triaxial test; (iii) consolidated undrained triaxial test; and (iv) consolidated drained triaxial test.

There were in total 6 drilling points, B1, B2, B5, B6, B9 and B10. From the laboratory tests results, the soil of the core is of CL to CL-ML soil, and the soil in the transition zone is of ML soil. The consolidated drained tests have been conducted for soil specimens obtained from boreholes B1 (upstream transition zone), B2 (core), and B6 (downstream transition zone). Their confining pressure varied between 100 and 400 kPa. The effective cohesion c' and effective friction angle ϕ' were obtained and presented in Table 1. The parameters for the shell region were taken from Chang et al (1996).

Table 1: Summary of soil parameters derived from laboratory tests.

Properties	B1 (upstream)	B2 (core)	B6 (downstream)
Dry density, γ_d (kN/m^3)	17.2	18.1	17.9
Young's modulus, E (MPa)	39.79	60.31	24.53
Poisson's ratio	0.45	0.46	0.45
Cohesion, c' (kPa)	90	100	55
Friction angle, ϕ' (degree)	30	31	24

SIMULATION OF RENYI-TAN DAM

Grid Generation

The first step of numerical analysis is to set up grids. Once the analysis starts, the grids cannot be changed until the end of the analysis. Figure 2 shows the mesh of dam with 1056-elements.

Boundary Conditions

The bottom boundary of the dam is extended 10 m below the base of the dam (Figure 2). The material at the foundation is clay, which is similar to the core area. The bottom boundary is fixed in x- and y-directions. The left and right boundaries of the foundation soil are fixed in x-direction, and free in y-direction. For water boundary, as water is stored at the upstream, the boundary below the water table is specified using the command FIX PORE PRESSURE to represent the water pressure, and FIX SATURATION to represent its saturation condition. Free-field boundary condition was also used in the analysis. In this way, plane waves propagating upward suffer no distortion at the boundary because the free-field grid supplies conditions that are identical to those in an infinite model (Itasca Consulting Group, Inc., 2002).

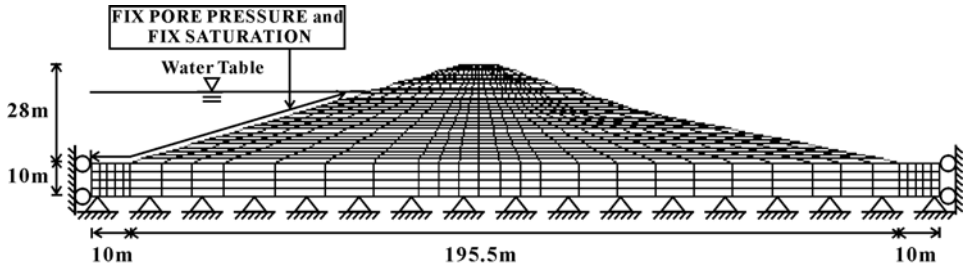

Figure 2. Grid used in FLAC2D (not to scale).

Flow Analysis

Flow analysis was performed to obtain the initial pore water pressure distribution in the dam. The full water storage height of the dam is 24 m. From the result of a pseudo static analysis it was found that as the water depth reduces, the FOS also reduces gradually until approximately half the water depth (12 m) where a further reduction in water depth would instead increase the FOS of the dam. Therefore, water tables of 12 m and 24 m have been chosen for the following analysis.

Earthquake History

In FLAC2D, dynamic input can be provided using acceleration history, velocity history, stress (or pressure) history, or a force history. Dynamic input is usually applied to the model boundaries with the APPLY command. In general, dynamic acceleration history can be determined using: (i) the accelerogram monitored during an earthquake; (ii) the artificially generated accelerograms; and (iii) a modified accelerogram that is obtained from (1) or (2). This study uses the first method. An ML = 5.0 earthquake was observed by an accelerometer some 2 km away from the Renyi-Tan Dam. Figure 3 shows the acceleration history.

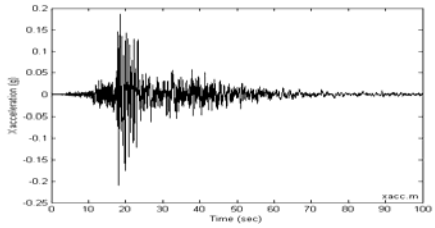

Figure 3. Acceleration history used in the dynamic analysis.

Rayleigh Damping

A dynamic numerical analysis must consider the energy loss or damping. Rayleigh damping is usually used in the analysis of structures and elastic continua to damp the natural oscillation modes of system. Rayleigh damping is normally represented using a damping matrix [*C*] with components proportional to the mass [*M*] and stiffness [*K*] matrices (Itasca Consulting Group, Inc., 2002):

$$[C] = \alpha[M] + \beta[K] \tag{7}$$

where α = the mass-proportional damping constant; and β = the stiffness-proportional damping constant. For a multiple degree-of-freedom system, its critical damping ratio ξ_i at any angular frequency ω_i may be related using equations (Bathe and Wilson, 1976):

$$\alpha + \beta\omega_i^2 = 2\omega_i\xi_i \qquad or \qquad \xi_i = \frac{1}{2}\frac{\alpha}{\omega_i} + \beta\omega_i \tag{8}$$

By setting $\alpha = 0$ or $\beta = 0$, we obtain:

$$\alpha = \omega_{\min}\xi_{\min} \quad or \quad \beta = \frac{\xi_{\min}}{\omega_{\min}} \tag{9}$$

where ω_{min} = the minimum angular frequency; and ξ_{min} = the minimum critical damping ratio. The minimum frequency is defined as:

$$f_{\min} = \frac{\omega_{\min}}{2\pi} \tag{10}$$

In FLAC, the damping parameters include both the values of f_{min} and ξ_{min}. For geological materials, critical damping ratio commonly falls in the range of 2% to 5% (Biggs, 1964) and this study uses 5%. For f_{min}, if a wavelength for the fundamental mode of a particular system can not be estimated, then a preliminary run may be made with zero damping (Itasca Consulting Group, Inc., 2002). A representative natural period may be estimated from time histories of velocity or displacement. f_{min} is derived from the power spectrum (Itasca Consulting Group, Inc., 2002). There are several definitions for a power spectrum. The one used here is adapted from Press et al. (1992). The power spectrum is a set of *N/2* real numbers defined as:

$$P_0 = \frac{1}{N^2}\left(|f_0|\right)^2; \qquad P_k = \frac{1}{N^2}\left[\left(|f_k|\right)^2 + \left(|f_{N-k}|\right)^2\right], \quad and \quad P_{N/2} = \frac{1}{N^2}\left(|f_{N/2}|\right)^2 \tag{11}$$

where N = half the number of points in the original data field; P = the power spectrum output; f = the result of the Fast Fourier Transform of the original data; and k = varies from 0 to *N/2*. Using this method, the minimum frequency f_{min} of 7.15 Hz has been observed and used in all the subsequent analyses.

RESULTS AND DISCUSSIONS

This section presents the results of the dynamic analysis of Renyi-Tan dam. The results are presented in the forms of displacement, pore water pressure, and acceleration.

Relative Displacement

The sequential displacement results below 12 m and 24 m of water tables are shown in Figure 4 and Figure 5, respectively. It can be seen that the global displacement is influenced by the height of water tables, and that the maximum displacement contour is generated between t = 20 and 30 sec, coincides with the main earthquake strike. After the main strike, no further displacement was seen generated (Figure 4(c) and Figure 5(c)).

It can be seen that the displacement of the upstream slope below 12 m of water table is greater than the displacement under 24 m of water table, whereas both the displacement of the downstream slope are similar for 12 m and 24 m of water table (Figure 4(d) and Figure 5(d)). This is because the hydrostatic water pressure is acting as a restoring pressure to the stability of the upstream slope. Therefore, the maximum displacement recorded for 24 m water table is only 2 cm compared to 4 cm in the case of 12 m water table. For the downstream slope the conditions are not affected by the 12 and 24 m water tables as it was always dry, it thus produced the same displacement contour. Thus the upstream slope under 12 m of water table is more unstable compare to the case of 24 m of water table; the stability result is similar to the result obtained using the pseudo static analysis (Gui and Wu, 2003).

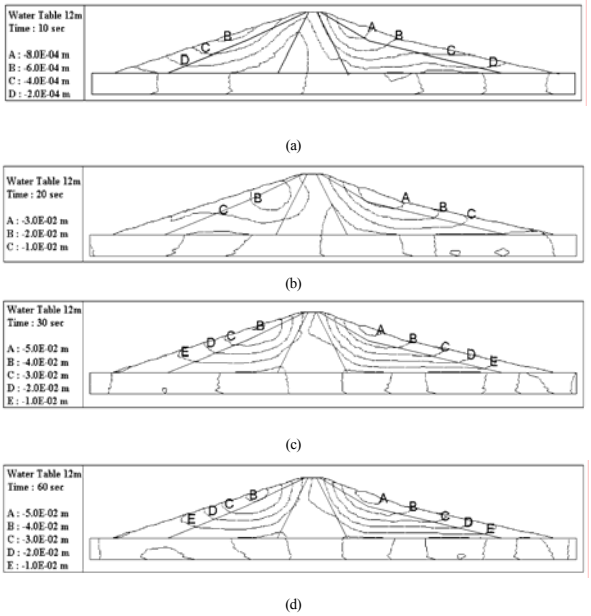

Figure 4. Contours of displacement under 12 m of water table: (a) at 10 sec; (b) at 20 sec; (c) at 30 sec; (d) at 60 sec.

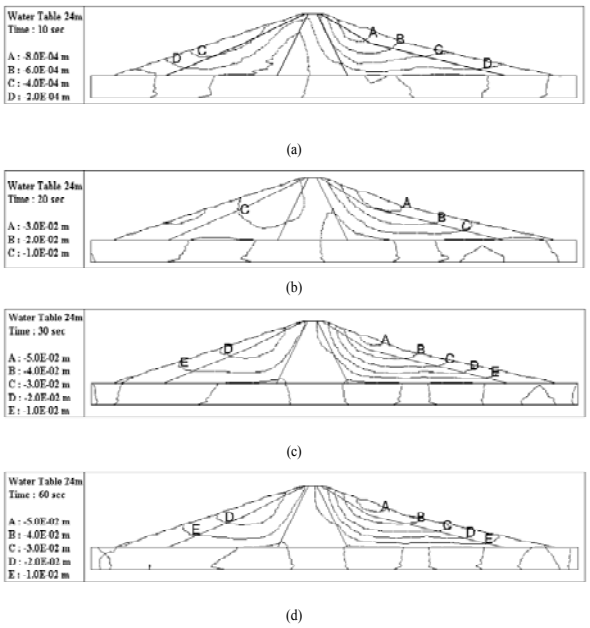

Figure 5. Contours of displacement under 24 m of water table: (a) at 10 sec; (b) at 20 sec; (c) at 30 sec; (d) at 60 sec.

Pore Water Pressure

Figure 6 and Figure 7 show the pore water pressure contours generated below 12 m and 24 m of water tables. From these plots, it was observed that the pore water pressure increases with the increased of earthquake acceleration. Again, the maximum pore water pressure was generated between t = 20 and 30 sec. As expected, the pore water pressure generated under 24 m of water table is higher than the pore water pressure generated under 12 m of water table (Figure 6(d) and Figure 7(d)). This is because the initial pore water pressure under 24 m of water table is already higher than the initial pore water pressure under 12 m of water table. It is interesting to note that the zone of maximum pore water pressure is located at the base of the upstream transition zone (Figure 6(c) and Figure 7(c)). This finding coincides with the results presented by Ming and Li (2003) that employed finite element program to analyze the San Fernando dam.

Excess pore water pressure may be generated in sand during an earthquake shaking. If the excess pore water pressure is greater than the effective stress of the soil, liquefaction occurs, and it leads to soil failure since soil can no longer sustain loading. Figure 8 shows the ratio of excess pore pressure generated and initial effective stress in the upstream transition zone. The ratio is defined as the ratio of excess pore water pressure and initial effective overburden stress. In the upstream transition zone, the recorded values for the excess pore water pressure ratio vary from location to location with a maximum ratio of about 62% (under 24 m of water table) recorded by PPT1 near the upstream shell and the base of the transition zone. In general, the excess pore water pressure ratio for 24 m of water table was seen higher than the ratio for 12 m of water table. This is because in order to preserve the total stress, a soil element at some depth *z* with a small effective vertical stress must generate an excess pore water pressure value that equals the difference between its total and effective vertical stresses. At locations of PPT1, PPT2, PPT3 and PPT4, their respectively effective vertical stresses are higher in the case of 12 m water table than the 24 m water table. Therefore, to preserve the total stress at these locations, soil elements in the case of 24 m water table must generate a higher excess pore water pressure than in the case of 12 m water table. The excess pore water pressure generated quickly during the main earthquake, and is accumulated in such a way as described by the Finn model.

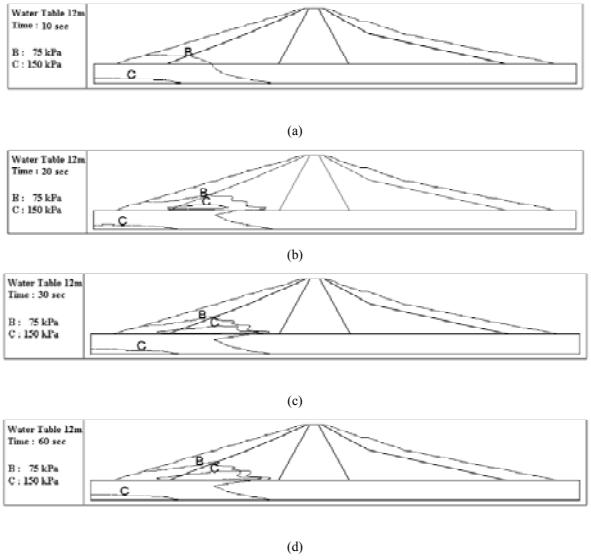

Figure 6. Pore water pressure contours under 12 m of water table: (a) at 10 sec; (b) at 20 sec; (c) at 30 sec; (d) at 60 sec.

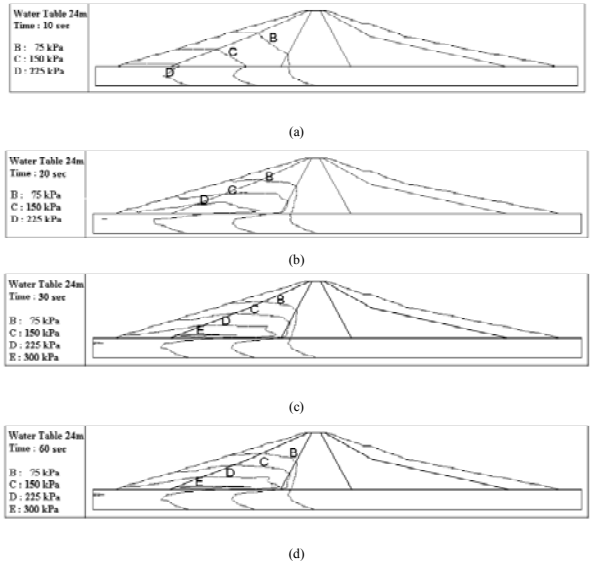

Figure 7. Pore water pressure contours under 24 m of water table: (a) at 10 sec; (b) at 20 sec; (c) at 30 sec; (d) at 60 sec.

Acceleration

During earthquake shaking, the influence of soil characteristics, soil thickness, and earthquake wavelength might magnify the earthquake acceleration (Shunzo Okamoto, 1984). This is especially so for the trapezoidal shaped structure such as dam where the acceleration is magnified as it propagates from the base to the top of the dam. The acceleration history at various location of the dam during shaking is recorded and compared in this section. Figure 9 shows the results of acceleration history in the upstream shell, upstream transition zone, core, downstream transition zone, and downstream shell.

Magnification factor can be obtained by dividing the maximum acceleration at any depth with the maximum acceleration at the base of the foundation or the input acceleration. As earthquake travels from the base of foundation to the top of the dam, the magnification factor increases. Magnification occurs as soon as it begins propagation at the base of the foundation, probably because of the material used for the foundation and the core area. The maximum input acceleration was 0.22g while the recorded maximum acceleration at the top of the dam was 0.50g, thus a magnification factor of 2.3 is obtained for the Renyi-Tan dam during the 921-earthquake.

CONCLUSIONS

From the results of the dynamic analysis, when water table is 12 m, the upstream slope generates a 4 cm displacement, and the downstream slope generates a 5 cm displacement. When water table is 24 m, the upstream slope generates a 2 cm displacement, and the downstream slope generates a 5 cm displacement. Therefore, we can see that a lower upstream water table corresponded to a larger slope displacement. As there is no water at the downstream slope in both cases the results of the downstream displacements are the same, irrespective to the upstream water table.

From the results of dynamic analysis, excess pore water pressure would be generated in saturated zones of the dam. The analysis shows that during shaking excess pore water pressure would be generated in especially near the bottom-left corner of upstream transition zone, which was also observed by Ming and Li (2003) who analyzed the failure of the San Fernando dam. In the upstream transition zone, because the material is of low plasticity silt, excess pore pressure is generated. The maximum ratio of excess pore water pressure obtained is about 62% under 24 m of water table. In the core zone, because there is not much water flowing in this area, there is only a small fraction of excess

pore water pressure is generated. In the upstream shell, which is mainly gravel, excess pore pressure is least generated.

During earthquake shaking, the earthquake acceleration is magnified as it propagates from the base to the top of the dam. Magnification factor is obtained by dividing the maximum acceleration at any depth with the maximum acceleration at the base of the foundation or the input acceleration. It was found that magnification occurs as soon as it propagates up from the base of the foundation.

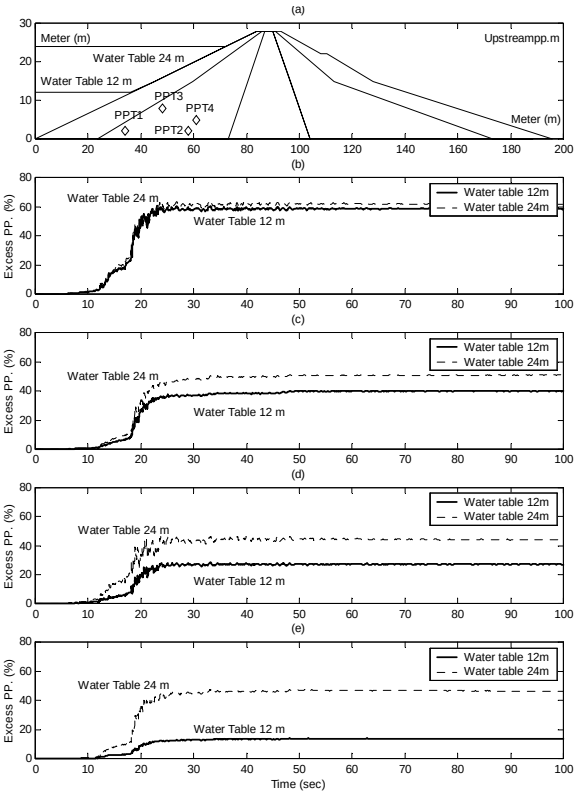

Figure 8. Ratio of excess pore water pressure in upstream transition zone: (a) sectional drawing of Renyi-Tan dam; (b) at PPT1; (c) at PPT2; (d) at PPT3; (e) at PPT4.

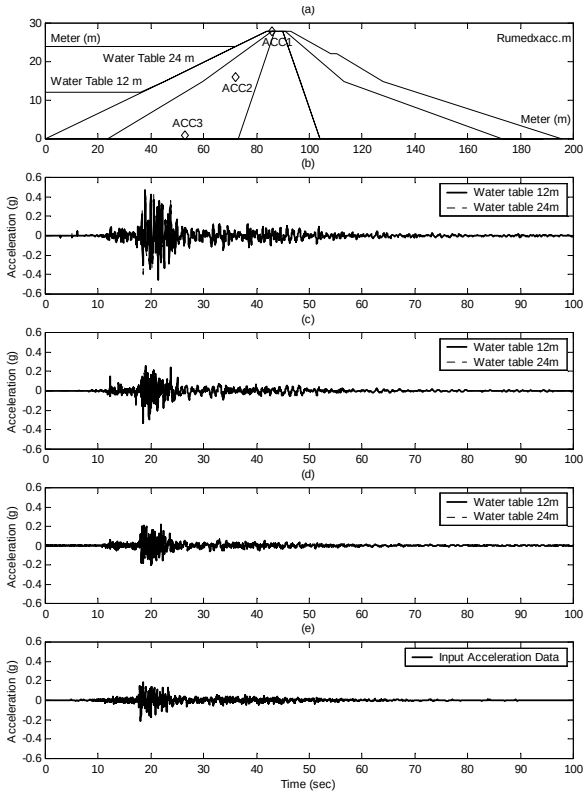

Figure 9. Accelerative history in the upstream transition zone: (a) sectional drawing of Renyi-Tan dam; (b) at ACC1; (c) at ACC2; (d) at ACC3; (e) input acceleration.

ACKNOWLEDGMENTS

The authors are grateful to the financial support provided by the National Science Council of ROC under the research agreement NSC91-2211-E-027-009.

REFERENCES

Bathe, K.J. and Wilson, E.L. (1976). *Numerical Methods in Finite Element Analysis*, Prentice-Hall, Inc., Eaglewood Cliffs, New Jersey.

Biggs, J.M. (1964). *Introduction to Structural Dynamics*, McGRAW-Hill Book Co.

Chang, Chi-Tso, Chen, Yit-Jin, Yen, Shih-Chieh, and Chai, Yi-Chang (1996). "Study of engineering properties and construction method for gravel formations in central and northern Taiwan." *Sino-Geotechnics*, **55**, 35-46. (in Chinese).

Gui M W & Wu H H (2003). "Seismic analysis of Renyi dam in Taiwan." *Proc 12th Asian Regional Conf. on Soil Mechanics and Geotechnical Engineering, Singapore,* 287-290.

Hsu, Sung-Chi, Chu, Bin-Lin and Lin, Chen-Chuan (2003). "Study of lateral spreading in Wufeng during 921-JiJi Earthquake." *Proc. 10th Taiwan Geotechnical Engineering Conference*, 893-896

ICOLD (1979). *World Register of Dams, 2nd Updating*. International Commission on Large Dams, Paris.

Itasca Consulting Group, Inc. (2002). FLAC User Manual: Version 4.0. USA..

Lee, Chia-Han (2001). Numerical modeling of earthquake-induced liquefaction of backfill behind caisson type quay walls. *Master Degree Dissertation,* National Central University, Taiwan. (in Chinese).

Martin, G.R., Finn, W.D.L., and Seed, H.B. (1975). "Fundamentals of Liquefaction under Cyclic Loading." *Journal of Geotechnical Engineering Division*, ASCE, **101**(5), 423-438.

Ming, H.Y., and Li X.S. (2003. "Fully Coupled Analysis of Failure and Remediation of Lower San Fernando Dam." *Journal of the Geotechnical and Geoenvironmental Engineering*, ASCE, **129**(.4), 336-349.

NTIT (1987). *Soil Testing Report for Renyi-Tan Dam Earth-filled Materials.* National Taiwan Institute of Technology. (in Chinese).

Press et al. (1992)

Rizendiz, D., Romo, M. P. and Moreno, E. (1982). "E1 Information and La Villita Dams: Seismic Behavior", *J. Geotechnical Engineering, Div.* ASCE, **108**(1), 109-131.

Seed, H. B., Makdisi, F.I. and De Alba, P.(1977). The Performance of Earth Dams During Earthquakes, *Report No.EERC-77/20, EERC*, Univ. of California, Berkeley.

Silver, M.L., and Seed, H.B. (1971). "Volume Changes in Sands during Cyclic Loading." *Journal of the Soil Mechanics and Foundations Division*, ASCE, **97**(9), 1171-1182.

Shunzo Okamoto (1984). *Introduction to Earthquake Engineering*. University of Tokyo Press, 2nd ed., 630p.